Title

Observation of multi-channel non-local transport in J-TEXT plasmas

Journal

Nuclear Fusion, 58(4)

ISSN

0029-5515

Authors

Shi, Yuejiang
Chen, Zhongyong
Yang, Zhoujun
et al.

Publication Date

2018-04-01

DOI

10.1088/1741-4326/aaaa9b

Observation of multi-channel non-local transport in J-TEXT plasmas

Yuejiang Shi[1*], Zhongyong Chen[2], Zhoujun Yang[2], Peng Shi[2], Kaijun Zhao[3*], Partick H Diamond[3,4], JaeMin Kwon[5], Wei Yan[2], Hao Zhou[2], Xiaoming Pan[2], Zhifeng Cheng[2], Zhiping Chen[2], SeongMoo Yang[1], Chi Zhang[2], Da Li[2], Yunbo Dong[3], Lu Wang[2], YongHua Ding[2], Yunfeng Liang[2,6], SangHee Hahn[5], HoGun Jhang[5], Yong-Su Na[1]

[1]Department of Nuclear Engineering, Seoul National University, Seoul, Korea

[2]College of Electrical and Electronic Engineering, Huazhong University of Science and Technology, Wuhan, China

[3]Southwestern Institute of Physics, Chengdu, China

[4]CMTFO and CASS, University of California, San Diego, USA

[5]National Fusion Research Institute, Daejeon, Korea

[6]Forschungszentrum Jülich GmbH, Institut für Energie-und Klimaforschung-Plasmaphysik, Partner of the Trilateral Euregio Cluster (TEC), Jülich, Germany

[*]*E-mail of corresponding author: yjshi@ipp.ac.cn and kjzhao@swip.ac.cn*

Abstract. In cold pulse experiments in J-TEXT, not only are rapid electron temperature increases in core observed, but also steep rises of inner density are found. Moreover, some evidence of acceleration of the core toroidal rotation is also observed during the non-local transport process of electron temperature. These new findings of cold pulse experiments in J-TEXT suggest that turbulence spreading is possible mechanism for the non-local transport dynamics.

There are several outstanding experimental mysteries in magnetic fusion plasma research. A fast increase of the central electron temperature caused by the edge cooling in ohmic heating plasmas, the so-called non-local heat transport (NLT) [1] is one of these challenging issues. NLT was first observed in the TEXT tokamak 22 years ago, and in many fusion devices afterwards [2-12]. NLT phenomenon shows that the limitation of transport theory based on a local transport model. The underlying physics mechanism of NLT is still unclear.

One typical characteristic of NLT is this effect disappears with increasing electron density. The critical density where the NLT effect disappears is defined as cutoff density. The experimental results from C-mod [9, 10] and KSTAR [12] show the close correlation between the cutoff density of NLT and the plasma confinement status. In C-mod Ohmic heating plasmas [9,10], NLT can be achieved in linear Ohmic confinement (LOC) plasma with relative lower density and disappears in saturated Ohmic confinement (SOC) plasma with relative higher density. In KSTAR plasmas [12], the cutoff density of NLT can be can be significantly increased by electron cyclotron resonance heating because the transition density in ECH plasma from linear to saturated confinement is much higher than the density for LOC-

SOC transition. The experimental behaviors of cutoff density of NLT looks consist with the some prominent theoretical hypotheses based on turbulence theory [13-17].

On the other hand, the latest experimental results in J-TEXT tokamak show a steep rises of core density and acceleration of core rotation, which are accompanied by rapid electron temperature increases. These simultaneous increments in three confinement channels are found for the first time in experimental fusion plasmas. The new experimental findings of non-local transport in J-TEXT in this paper provide a key clue to reveal more clear background physics mechanism for NLT. All the results presented in this paper are obtained from J-TEXT tokamak [18].

The major radius of J-TEXT is 1.05m. The minor radius of J-TEXT is 0.255m in this experiment. All the discharges are OH heating plasmas with circular limiter configuration. In J-TEXT, the electron temperature (T_e) is measured with the electron cyclotron emission radiometer (ECE) [19]. At the same time, the fluctuation of T_e for core plasma is measured with correlation electron cyclotron emission radiometer (CECE) [20]. A 17-channel polarizer-interferometry system (POLARIS) [21] which covers the whole region of J-TEXT plasma from high field side to low field side, measures the electron density (n_e). The x-ray crystal spectrometer (XCS) [22] provides core toroidal rotation velocity. Multi-pulse supersonic molecular beam injection (SMBI) [23] is applied as cold pulse source to trigger NLT in J-TEXT [24]. The toroidal magnetic field (B_T) is fixed at 1.8T, which make the best spatial measured coverage of ECE.

Fig.1 shows the waveforms of a representative OH discharge with five SMBI cold pulse injection in J-TEXT. The pulse duration of SMBI is 0.3ms. The time interval between each SMBI pulse is 50ms i.e. 20Hz modulation frequency. The plasma current (I_p) and edge safety factor (q_a) are 150kA and about 3.7, respectively. The cutoff density (line averaged value) for NLT in J-TEXT with B_T = 1.8T and I_p=150kA is about $2.3\times10^{19}m^{-3}$. The typical NLT effect in electron channel (core T_e rise while edge T_e drops) appears in every SMBI pulse, which is same as previous NLT experiments in other devices [1-12]. On the other hand, the prompt increasing of line-averaged density due to SMBI is clear shown in fig.1a. However, the line-average density includes the contributions from edge and core region. More accurate characters for the particle transport during NLT should be acquired from the local density response and profiles. Both time and spatial information of local electron density can be obtained from the 17-ch line integrated density of POLARIS with matrix inversion technique.

The detail time evolution of the core density (n_{e0}) during the first SMBI pulse in fig.1 is shown in fig.2a. Fig.2b shows the evolution of profiles of T_e and n_e during the first SMBI pulse in fig.1. Obviously, there are two different time scale for the evolution of n_{e0}. One is the steep rise of n_{e0} in serval milliseconds in the beginning. The other is the slow increase and sustainment in the following tens milliseconds. Moreover, the steep rise of n_{e0} is synchronous with the fast increase of T_{e0}. For the J-TEXT SMBI experiments, the neutral penetration of SMBI mainly concentrated in the SOL and plasma edge region (r>23cm) [25]. If the steep rise of n_{e0} is caused by local transport process, the averaged convection velocity from edge to core should be more than 40 m/s (~0.2m/5ms). On the other hand, the spatial particle transport coefficients based on perturbation principle and modulation technology [26-33] also can be calculated for the 5-pulse SMBI plasma in fig.1. The detail analysis technique for particle transport coefficients based on the local density profile can be found in ref.32. The modulated amplitude and phase of local density are shown in fig.3a and fig.3b. The profiles of diffusion and convection velocity are shown in fig.3c and fig.3d. The convection velocity at r/a=0.75 reaches 90m/s. Normally, the particle convection velocity in other machines [26,27,33] which are similar size as J-TEXT is around 1~10m/s , which is already much higher than the neo-classic prediction (abnormal transport). Compared to experiment results of other machines, both averaged 40m/s and localized 90m/s, which are estimated from local transport mode, are astounding high value. Similar to the fast rise of T_{e0}, the steep rise of n_{e0} should be also caused by some non-local transport process.

Now, we turn the focus in fig.1 again. One notable point in fig.1 is the sawtooth period ($\tau_{sawtooth}$ in fig.1b) also clearly increases for the all the 5 SMBI pulses. And the increasing pace of $\tau_{sawtooth}$ is coincident with the core T_e rise. The increasing of $\tau_{sawtooth}$ has high possible correlation with the acceleration of core toroidal rotation, which will be demonstrated by the following section.

There are two plasma parameters can affect the $\tau_{sawtooth}$ of J-TEXT's plasmas with fixed I_P and B_T. One is electron density, and the other is toroidal rotation velocity. Fig.4a shows the waveforms of one density ramping-down discharge. I_P and B_T in shot no. 1049889 in fig.4a are same value as those in shot no. 1049867 in fig.1. It can be seen in fig.4a that the $\tau_{sawtooth}$ decreases with decreased $\overline{n_e}$. On the other hand, the core V_ϕ also increases with density as shown in fig.4a. The time trace of V_ϕ is available in limited time period in fig.4a because the measurements of XCS are seriously disturbed by some mechanical vibration in later time

period in this discharge. Here, we note that the core V_ϕ measured with XCS is always in counter-current direction in our experiments on J-TEXT. In this paper, the negative sign for V_ϕ or ΔV_ϕ means that the rotation velocity or rotation acceleration is in counter-current direction. It is hard to say from fig.4a which one is dominant factor to affect $\tau_{sawtooth}$. Tangential neutral beam injection (NBI) is a very useful tool to actively control V_ϕ. Although there is no NBI in J-TEXT at present, the resonance magnetic perturbation coils (RMP) in J-TEXT [34] is also a powerful actuator to change V_ϕ. Fig.4b shows the waveforms of one discharge (shot no. 1049965) with application of RMP at the same B_T and I_p as those in fig.4a and fig.1. It can be seen that the changing amplitude of $\overline{n_e}$ during the second RMP pulse injection period in fig.4b is much small than that in fig.4a. It is very clear in fig.4b that $\tau_{sawtooth}$ increase with V_ϕ.

The correlation between the toroidal rotation and sawtooth activity has been reported both in experimental paper [35-39] and theoretical paper [39, 40]. On the other hand, the effects of density on sawtooth period have also been verified on several devices [41-43]. Here, we don't discuss which one (n_e or V_ϕ) is more dominant factor to affect $\tau_{sawtooth}$ in J-TEXT in this paper. We just simply assume both $\overline{n_e}$ and V_ϕ can affect $\tau_{sawtooth}$. Fig.5a and Fig.5b shows the scaling relation of $\overline{n_e}$ v.s. $\tau_{sawtooth}$ and V_ϕ v.s. $\tau_{sawtooth}$. It can be seen that $\tau_{sawtooth}$ has linear relation with $\overline{n_e}$ and 2nd order polynomial relation with V_ϕ within certain range. In fig.1, the increasing amplitude of $\tau_{sawtooth}$ ($\Delta\tau_{sawtooth}$) is about 0.25ms after SMBI injection. According to the scaling relation in Fig.5a, the increasing amplitude of ($\Delta\overline{n_e}$) should be about $0.22\times10^{19}m^{-3}$ to make corresponding $\Delta\tau_{sawtooth}$. The real experimental $\Delta\overline{n_e}$ after SMBI injection is only about $0.1\times10^{19}m^{-3}$, which is much lower than the estimated value from the scaling relation in Fig.5a. Moreover, $\tau_{sawtooth}$ already decreases while $\overline{n_e}$ still sustains high level for serval ten milliseconds. So the effect of $\overline{n_e}$ can be excluded for the prompt change of $\tau_{sawtooth}$ in fig.1. Now V_ϕ is the one possible parameter to make the rapid change of $\tau_{sawtooth}$ after SMBI injection in fig.1. According to the scaling relation in fig.5b, the increasing amplitude of V_ϕ should be around -1.4km/s to make corresponding $\Delta\tau_{sawtooth}$. Unfortunately, the XCS in J-TEXT at present cannot catch the fast time scale of NLT and the small changing amplitude of V_ϕ. More directly evidence of corresponding response of V_ϕ during NLT will be confirmed if the performance of related diagnostics can be greatly improved in the future.

Not only are the rapid electron temperature increases in core observed in J-TEXT cold pulse experiments, but also the steep rises of inner density and possible acceleration of core toroidal rotation are found. The J-TEXT results are the first experimental discovery of simultaneous fast NLT responses in multi-channels transport (electron temperature, particle, and momentum) in magnetic fusion plasma. Turbulence spreading [44-48] is the possible mechanism to explain the multi-channel NLT dynamics. The fast inward particle pinch induced by turbulence spreading [48] may explain the rapid increases of core density. The fast increases of electron temperature and acceleration of core rotation are also qualitatively predicted with the latest numerical simulation based on turbulence spreading theory [15].

The main idea to explain NLT dynamic in cold pulse experiment with turbulence spreading is as following. The turbulence is triggered by cold pulse in the outer unstable linear plasma and propagates to the core with very fast spreading process. The core part of LOC plasma is below marginal stability and provides room for further performance improvement until the SOC is reached. The local fluctuation intensity is depleted during turbulence spreading process from edge to core, which provides some free energy to steepen up the gradient of macroscopic parameters (temperature, density, etc.) in core region. The fluctuation information of electron temperature of core region (r/a=0.18) from CECE for the shot in fig.1 is shown in fig.6. It can be seen in the autopower spectrum of CECE (fig.6a) that the low frequency fluctuation (f<10 kHz) of T_e is dominated by some coherence mode. The relative high frequency fluctuation (20 kHz<f<100 kHz) with f^{-1} dependence show the typical turbulence characters. The behavior of autopower spectrum of electron temperature fluctuation is quite general. On the other hand, the crosspower spectra of CECE in fig.6b show some unique characters at multi-scale frequency domain. Firstly, the intensity of crosspower at about 1kHz increases during NLT period. Actually, the fluctuation at 1 kHz is mainly related to sawtooth activity because the sawtooth period in this shot is around 1ms. Generally, the sawtooth amplitude or intensity increases with the sawtooth period for Ohmic heating plasma. So the enhanced crosspower at 1 kHz in fig.6b is consistent with the longer sawtooth period during NLT period in fig.1a. Secondly, the intensity of crosspower from 4 kHz to 10 kHz during NLT period clearly decreases. Thirdly, the intensity of crosspower from 20 kHz to 60 kHz obviously increases during NLT period. Obviously, the effects of relatively low frequency fluctuation (4 kHz to 10 kHz) on macroscopic confinement and transport should be much stronger than that of relatively high frequency fluctuation (20 kHz to 60 kHz). So the increment of core T_e during NLT should be attributed to reduction of fluctuation

intensity in these low frequency domains, which is also consisted with the turbulence spreading model. On the other hand, the enhanced intensity from 20 kHz to 60 kHz during NLT period indicates that the propagation of turbulence spreading maybe executed in these high frequency fluctuations.

Although turbulence spreading can qualitatively explain the NLT dynamics, the quantitative simulation compared with real experimental data is necessary and important to enhance the credibility of related theoretical hypotheses.

Acknowledgement

This research is supported by the BK21 Plus project and R&D Programs through National Research Foundation of Korea (NRF) funded by the Ministry of Science, ICT and Future Planning of the Republic of Korea (No. 2014M1A7A1A03045368, No. 21A20130012821, and NFRI-EN1741-3). This research is also supported by National Magnetic Confinement Fusion Science Program funded by Ministry of Science and Technology of China (No. 2014GB108001, 2015GB111002, and 2015GB12003) and National Natural Science Foundation of China (No. 11775089).

Reference

[1] K. W. Gentle *et al*, Phys. Rev. Lett. **74**, 3620 (1995).

[2] M. W. Kissick *et al*, Nucl. Fusion **36,** 1691 (1996).

[3] P. Mantica *et al*, Phys. Rev. Lett. **82**, 5048 (1999).

[4] F. Ryter *et al*, Nucl. Fusion **40** , 1917 (2000).

[5] X. L. Zou *et al*, Plasma Phys. Control. Fusion **42**, 1067 (2000).

[6] P. Mantica *et al*, Plasma Phys. Control. Fusion **44**, 2185 (2002).

[7] N. Tamura *et al*, Phys. Plasmas **12**, 110705 (2005).

[8] H. J. Sun *et al*, Plasma Phys. Control. Fusion **52**, 045003 (2010).

[9] J. E. Rice *et al*, Nucl. Fusion **53**, 033004 (2013).

[10] C. Gao *et al*, Nucl. Fusion **54**, 083025 (2014).

[11] K. Ida *et al*, Nucl. Fusion **55**, 013022 (2015).

[12] Y.J.Shi *et al*, Nucl. Fusion **57**, 066040 (2017).

[13] P.H. Diamond *et al*, Phys. Plasmas **15** 012303 (2008).

[14] V. Naulin *et al*, Rotation reversal in a 1D turbulence spreading model *Proceedings of the 41st EPS Conference on Plasma Physics: Europhysics Conference* (Berlin, Germany, 23-27 June 2014)Vol. **38F** P2.067, http://ocs.ciemat.es/EPS2014PAP/pdf/P2.067.pdf

[15] F. Hariri *et al*, Phys. Plasmas **23** 052512 (2016).

[16] J.M. Kwon *et al*, Nucl. Fusion **52** 013004 (2012).

[17] P.H. Diamond *et al*, Nucl. Fusion **53** 104019 (2013).

[18] G. Zhuang *et al*, Nucl. Fusion **51**, 094020 (2011).

[19] Z.J.Yang *et al*, Rev. Sci. Instru*m.* **87**, 11E112 (2016).

[20] Z.J.Yang *et al*, Rev. Sci. Instru*m.* **86**, 043501 (2015).

[21] J.Chen *et al*, Rev. Sci. Instrum. **85**, 11D303 (2014).

[22] J.Wei *et al*, Rev. Sci. Instrum. **83**, 10E502 (2012).

[23] L.H.Yao *et al*, Nucl. Fusion **38**, 631 (1998).

[24] J.S.Xiao *et al*, IEEE TRANSACTIONS ON PLASMA SCIENCE **41**, 3675(2013)

[25] J.S.Xiao *et al*, J Fusion Energ **34**, 1020 (2015).

[26] K. W. Gentle *et al*, Plasma Phys. Control. Fusion **29**, 1077(1987).

[27] K. W. Gentle *et al*, Nucl. Fusion **32**, 217 (1992).

[28] K. Nagashima *et al*, Nucl. Fusion **33**, 1677 (1993).

[29] J O'Rourke *et al*, Plasma Phys. Control. Fusion **35**, 585(1993)

[30] N.J. Lopes Cardozo, Plasma Phys. Control. Fusion **37**, 799(1995).

[31] D.R.Baker, *et al*, Nucl. Fusion **38**, 485(1998)

[32] H. Takenaga *et al*, Nucl. Fusion **40**, 183 (1998).

[33] K. Tanaka *et al*, Chin. Phys. Lett. **21**, 2458 (2004).

[34] B. Rao *et al*, IEEE TRANSACTIONS ON APPLIED SUPERCODUTIVITY, **22**, 4201804(2012)

[35] J.Kim *et al*, The Effect of Toroidal Plasma Rotation on Sawtooth Activity in KSTAR, *in Proceedings of the 24th International Conference on Fusion Energy, San Diego, USA,*

2012(IAEA, Viena, http://www-naweb.iaea.org/napc/physics/FEC/FEC2012/html/fec12.htm),

http://www-naweb.iaea.org/napc/physics/FEC/FEC2012/papers/616_EXP814.pdf

[36] S. Scarabosio *et al*, Plasma Phys. Control. Fusion **48**, 663(2006)

[37] B. P. Duval *et al*, Phys. Plasmas **15**, 056113 (2008)

[38] B. P. Duval *et al*, Momentum Transport in TCV Across Sawteeth Events, *in Proceedings of the 23rd International Conference on Fusion Energy, Daejeon, Korea,*2010(IAEA, Viena, http://www-naweb.iaea.org/napc/physics/fec/fec2010/html/fec10.htm) http://www-naweb.iaea.org/napc/physics/fec/fec2010/papers/exs_p4-01.pdf

[39] I.T. Chapman *et al*, Nucl. Fusion **46**, 1009 (2006).

[40] I.T. Chapman *et al*, Phys. Plasmas **13**, 062511 (2006).

[41] D.J.Campbell, *et al*, Nucl. Fusion **26**, 1085(1986).

[42] H.K.B.Pandya, *et al*, Plasma Phys. Control. Fusion **49**, 1809(2007).

[43] S.Nowak, *et al*, Nucl. Fusion **54**, 033003 (2014).

[44]X. Garbet *et al*, Nucl. Fusion **34**, 963 (1994).

[45] P.H. Diamond and T.S. Hahm, Phys. Plasmas **2**, 3640 (1995).

[46] T.S.Hahm *et al*, Plasma Phys. Control. Fusion **46**, A323 (2004).

[47] Ö.D. Gürcan *et al*, Phys. Plasmas **12**, 032303 (2005)

[48] V. Naulin, A. H. Nielsen and J. J. Rasmussen, Phys.Plasmas **12**, 122306 (2005)

Figures

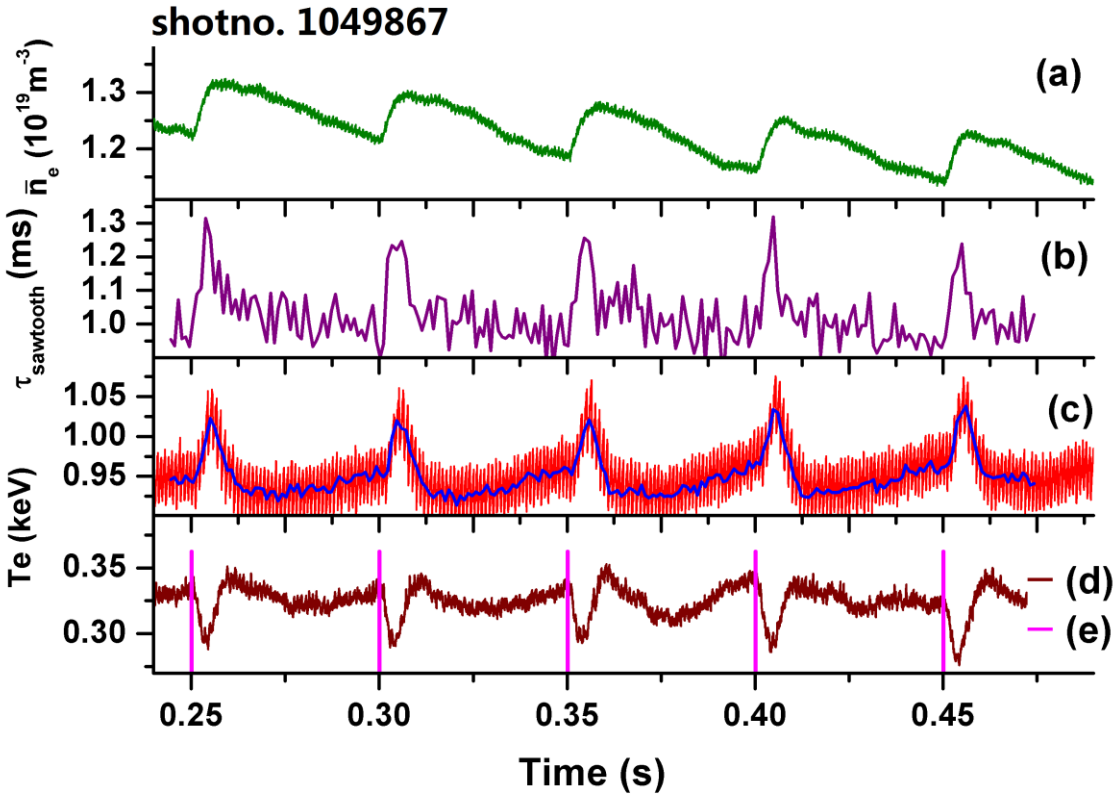

Fig.1 *The waveforms of cold pulse discharge with multi-pulse SMBI (shot no.1049867); (a) line-averaged electron density, (b) sawtooth period (c) core electron temperature, blue line is temperature at the middle time of each sawtooth cycle (d) edge electron density at r/a=0.79, and (e) SMBI pulse signal.*

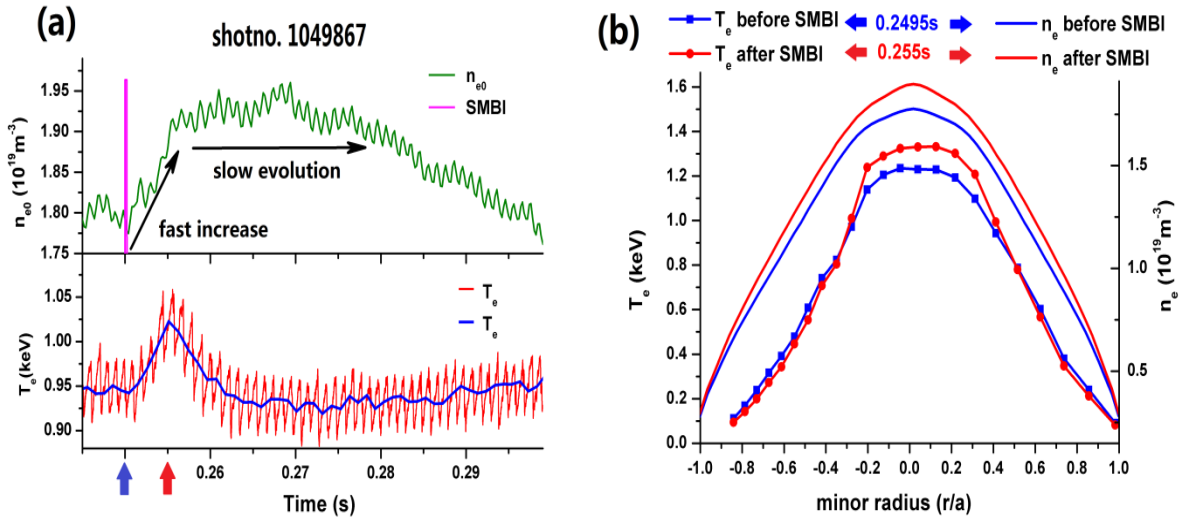

Fig.2a *The detail time evolution of core T_e and n_e for the first SMBI pulse in fig.1. The blue line represents T_e at the middle time of each sawtooth cycle*

Fig.2b *The profiles of T_e and n_e for the first SMBI pulse in fig.1.*

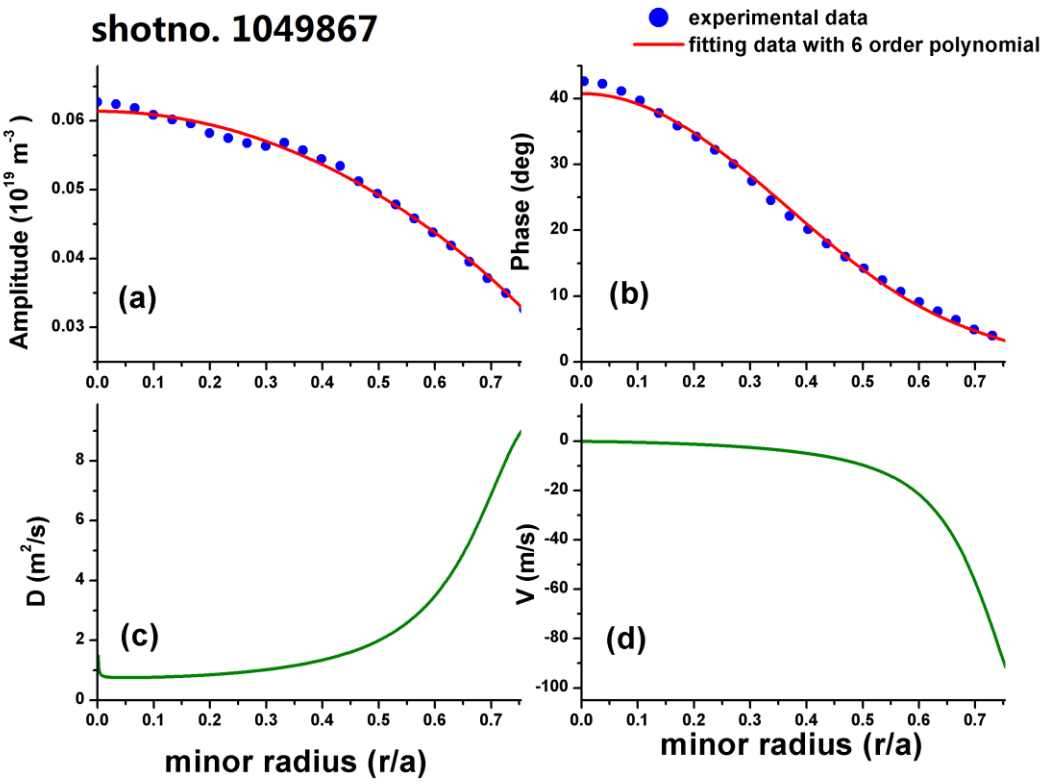

Fig.4 *Profiles of modulated amplitude (a) and phase (b) for the 5 SMBI pulses in fig.1*

Profiles of diffusion coefficient (c) and convection velocity (d) calculated based on perturbation principle.

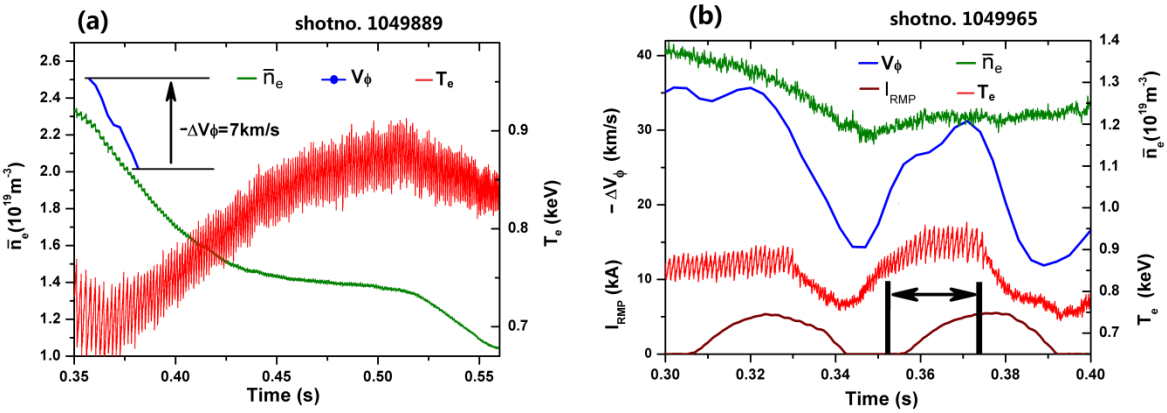

Fig.4a *The waveforms of density ramping-down plasma (shot no.1049889);*

Fig.4b *The waveforms of RMP plasma (shot no.1049965). The error bar of V_ϕ is about 3km/s.*

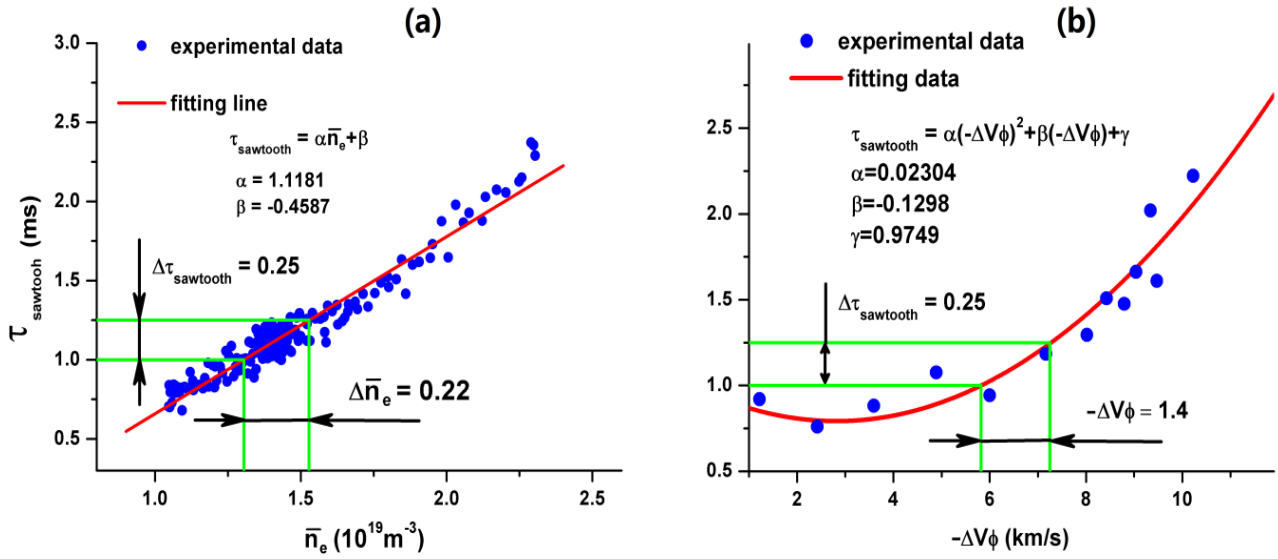

Fig.5a *The scaling relation between* $\overline{n_e}$ and $\tau_{sawtooth}$ *from the discharge (shot no.1049889) in fig.4a;*

Fig.5b *The scaling relation between* V_ϕ v.s. $\tau_{sawtooth}$ *from the discharge(shot no.1049965) in fig.4b. The data are taken from ramp-up phase of second RMP pulse (the time window is indicated by the black arrow in fig.3b).*

.

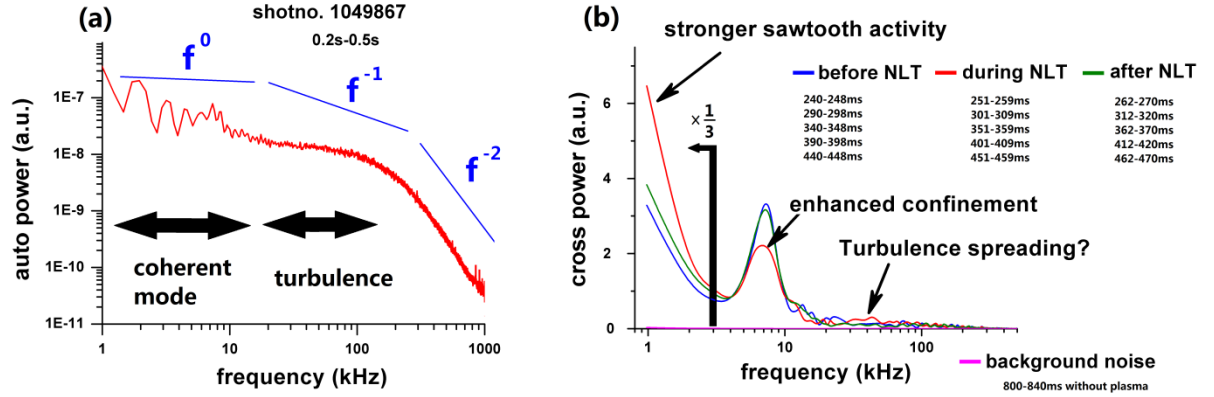

Fig.6 *(a) Autopower spectrum of one CECE channel located at r/a=0.18 for the shot in fig.1. The integrated time is 300ms. (b) Crosspower spectrum of two CECE channels at r/a =0.18. The integrated time for each crosspower spectrum is 40ms. The intensity of crosspower for f<3kHz is demagnified three times to make the behaviour of high frequency fluctuation more clear.*